Eur Biophys J (2008) 37:603–611
DOI 10.1007/s00249-008-0278-z

ORIGINAL PAPER

Complementing structural information of modular proteins with small angle neutron scattering and contrast variation

J. G. Grossmann · A. J. Callaghan · M. J. Marcaida · B. F. Luisi · F. H. Alcock · K. Tokatlidis

Received: 6 October 2007 / Revised: 18 January 2008 / Accepted: 22 January 2008 / Published online: 13 February 2008

Abstract Many macromolecules in the cell function by forming multi-component assemblies. We have applied the technique of small angle neutron scattering to study a nucleic acid–protein complex and a multi-protein complex. The results illustrate the versatility and applicability of the method to study macromolecular assemblies. The neutron scattering experiments, complementing X-ray solution scattering data, reveal that the conserved catalytic domain of RNase E, an essential ribonuclease in *Escherichia coli* (*E. coli)*, undergoes a marked conformational change upon binding a 5′monophosphate–RNA substrate analogue. This provides the first evidence in support of an allosteric mechanism that brings about RNA substrate cleavage. Neutron contrast variation of the multi-protein TIM10 complex, a mitochondrial chaperone assembly comprising the subunits Tim9 and Tim10, has been used to determine a low-resolution shape reconstruction of the complex, highlighting the integral subunit organization. It shows characteristic features involving protrusions that could be assigned to the six subunits forming the complex.

Keywords Small angle neutron scattering · Contrast variation · X-ray scattering · RNase E · Allosteric mechanism · TIM10

Abbreviations

SANS	Small angle neutron scattering
SAXS	Small angle X-ray scattering
RNase E	Ribonuclease E
TIM10	Translocase of the intermembrane space

Introduction

Small angle neutron scattering allows the isolation of scattering contributions of individual components within complex assemblies using the contrast variation method. For instance, the individual scattering contributions can be identified for the nucleic acid and protein in a nucleic acid–protein complex, or between deuterated and non-deuterated protein subunits within a multi-protein complex. This is achieved through manipulating the deuteration of the protein components and the deuteration level in the solvent such that the scattering density is matched to particular constituents of the multi-component systems. Scattering profiles obtained from contrast variation can be used to infer radii of gyration and to calculate molecular shapes. We

Advanced neutron scattering and complementary techniques to study biological systems. Contributions from the meetings, "Neutrons in Biology", STFC Rutherford Appleton Laboratory, Didcot, UK, 11–13 July and "Proteins At Work 2007", Perugia, Italy, 28–30 May 2007.

J. G. Grossmann (✉)
Molecular Biophysics Group, STFC Daresbury Laboratory,
Daresbury Science and Innovation Campus,
Warrington, Cheshire WA4 AD, UK
e-mail: j.g.grossmann@dl.ac.uk

A. J. Callaghan · M. J. Marcaida · B. F. Luisi
Department of Biochemistry, University of Cambridge,
80 Tennis Court Road, Cambridge CB2 1GA, UK

F. H. Alcock · K. Tokatlidis
Institute of Molecular Biology and Biotechnology,
Foundation for Research and Technology Hellas,
PO Box 1385, Heraklion, 71110 Crete, Greece

Present Address:
A. J. Callaghan
Biophysics Laboratories, Institute of Biomedical
and Biomolecular Science, University of Portsmouth,
King Henry Building, King Henry 1st Street,
Portsmouth PO1 2DY, UK

have applied this technique to study a nucleic acid–protein complex, namely the RNase E catalytic domain in equilibrium complex with an RNA substrate analogue, and a multi-protein complex involved in transmembrane transport in mitochondria.

Nucleic acid–protein complex study

RNase E is an essential hydrolytic endoribonuclease in *Escherichia coli* involved in the turnover of many, if not most, messenger RNA molecules. RNase E cleaves single-stranded substrates at A/U rich sites (McDowall et al. 1994). The ribonuclease preferentially cleaves substrates with a 5′ monophosphate over those with a 5′ OH or triphosphate group (Mackie 1998; Redko et al. 2003; Jiang and Belasco 2004). The crystal structure of the RNase E catalytic domain in complex with 5′ monophosphate–RNA substrate analogues revealed a compact tetrameric quaternary structure in which RNA binding sub-domains engulf the substrate and manoeuvre it into the active site (Callaghan et al. 2005) (Fig. 1a, b). The 5′ monophosphate is engaged in a recognition pocket, and it has been proposed that this protein–phosphate interaction triggers a conformational change in the enzyme that organizes the catalytic site and thus favors substrate cleavage (Callaghan et al. 2005) (Fig. 1c). However, currently there is no RNA-free structure to corroborate this hypothesis. We present evidence from small angle neutron scattering with contrast variation to show that the 5′ terminus of the RNA does indeed trigger a conformational change in RNase E catalytic domain. This change compacts the molecule, in agreement with the proposed allosteric model. These data are further supported by X-ray solution scattering studies.

Multi-protein complex study

The multi-component protein complex studied here is involved in protein translocation. Extensive protein translocation occurs in mitochondria where virtually all of the mitochondrial proteins are imported from the cytosol before being sorted within the body of the organelle. This event is orchestrated by distinct translocation machineries in the outer and the inner mitochondrial membranes (Pfanner and Geissler 2001). The TIM10 complex specifically chaperones the inner-membrane insertion of polytopic proteins such as ADP/ATP carrier (AAC) that delivers ATP to the rest of the cell. Hydrophobic proteins like the AAC are made in the cytosol where they are kept in a soluble state by chaperones. They are then targeted to outer membrane receptors, translocated across the mitochondrial outer membrane in an unfolded conformation, and finally inserted in the inner membrane by the specialised TIM22 translocase. To negotiate the aqueous divide of the space between the outer and inner membranes, they are specifically chaper-

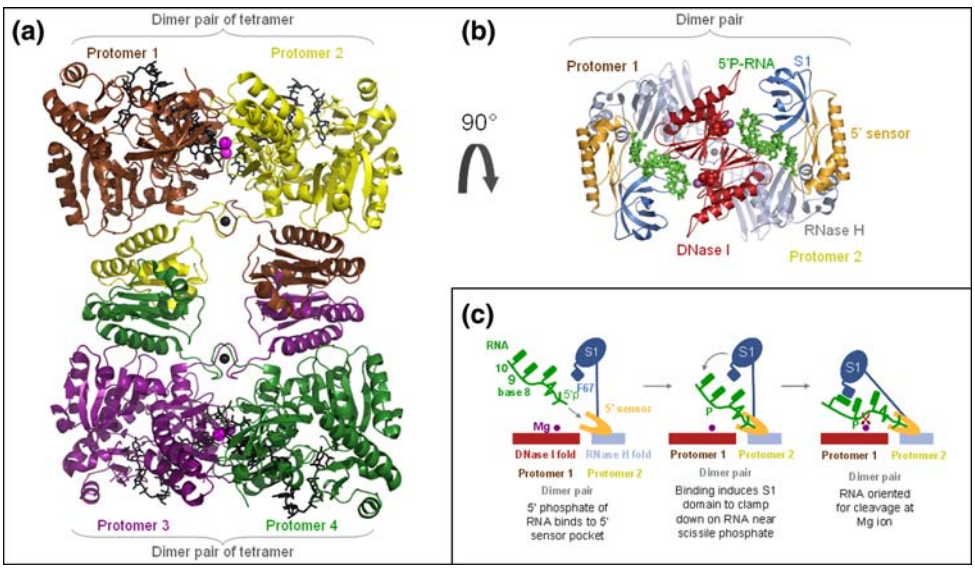

Fig. 1 5′ monophosphate RNA binding to RNase E catalytic domain. **a** Crystal structure of 5′ monophosphate–RNA-13-mer-bound RNase E catalytic domain. RNase E exists as a tetramer with one 5′ monophosphate–RNA 13-mer bound to each protomer. The individual protomers of the tetramer are labelled and coloured *brown*, *yellow*, *purple* and *green*, with bound 5′ monophosphate–RNA in *black*. The zinc and magnesium ions are shown as *black* and *magenta* spheres, respectively. The protomers comprising the dimer pairs within the tetramer are labelled. **b** Structure in (**a**) viewed from above and coloured according to subdomain structure. The DNase I subdomain is shown in *red*, the S1 domain in *blue*, RNase H fold in *grey* and 5′ sensor domain in *gold*. The protomers of the dimer illustrated are labelled. The subdomains are labelled for protomer two of the dimer pair. The 5′ monophosphate–RNA is in *green*. (**c**) Schematic model of the proposed mechanism of substrate cleavage. The model summarises RNase E's proposed conformational switch activated by binding RNA with a 5′ monophosphate. Figures were adapted from Callaghan et al. (2005)

oned by the TIM10 complex consisting of three Tim9 and three Tim10 proteins, each of about 10 kDa (Koehler et al. 1998; Curran et al. 2002; Vial et al. 2002). This complex does not utilise ATP hydrolysis and relies exclusively on conformational changes to perform its function. Solution X-ray scattering experiments allowed for the first time the size and molecular envelope of the complex to be determined (Lu et al. 2004). With a largest dimension of 70–80 Å, this could span at least half of the intermembrane space thereby 'shielding' the hydrophobic precursor from the aqueous environment. This low-resolution structure (based on threefold symmetry constraints) revealed characteristic features involving two classes of protuberances that could be assigned to the six subunits which make up the complex and might have specific functions in terms of substrate recognition (the substrate also has a triple internal repeat of a structurally related motif). In this study, we used contrast variation to obtain structural information on the individual subunits as part of the protein assembly. These data indicate that the component proteins Tim9 and Tim10 have very similar conformations within the TIM10 complex.

Experimental

Protein expression, purification and preparation for neutron scattering experiments

RNase E catalytic domain, encompassing residues 1–529 of *E. coli* full length RNase E was expressed and purified as described previously (Callaghan et al. 2003, 2005). RNA bound samples were prepared by mixing RNase E catalytic domain with equimolar RNA 10-mer substrate analogue, gel filtered into buffer (20 mM Tris–HCl pH 7.9, 500 mM NaCl, 10 mM DTT, 10 mM $MgCl_2$, 0.5 mM EDTA), and concentrated with centrifugal concentrators. Samples of complex with D_2O at 43 and 72% were prepared at 645 μM. A reference specimen without D_2O was prepared at a concentration of 370 μM in complex. The RNA used was 2′*O*-methyl protected of sequence ACAGUAUUUG, with either a 5′P or 5′OH incorporated. The 2′*O*-methyl modification prevents turnover of the substrate.

Tim9, one of the two essential translocases for inner membrane proteins (Tim9 and Tim10) that forms part of the *S. cerevisiae* TIM10 complex, has been expressed in deuterated form at the ILL-EMBL-PSB Deuteration Laboratory in Grenoble, France. The partner of Tim9, Tim10, was expressed in unlabelled form. Both proteins were expressed with a 6-His tag, and purified by nickel affinity chromatography according to published protocols (Vergnolle et al. 2007). Subsequently, a functional complex was formed between deuterated Tim9 and hydrogenated Tim10; purified and dialysed against buffers of 40 and 100% D_2O/H_2O mixtures for neutron scattering studies.

Neutron solution scattering

Small angle neutron scattering (SANS) experiments were carried out at beamline D22 of the Institut Langevin-Laue (ILL), Grenoble, France, providing neutrons of a wavelength of 6 Å (±10%) and using sample-to-detector distances between 2 and 5 m with collimator configurations of 8.2 and 5.6 m, respectively, so as to cover a q range between $q_{min} = 0.01$ Å^{-1} and $q_{max} = 0.45$ Å^{-1}. The magnitude of the scattering vector q is defined as $q = 4\pi \sin\Theta/\lambda$ where λ is the neutron wavelength and 2Θ is the scattering angle. The total counting time per sample was between 30 min and 2 h depending on the concentration (ranging from 3 to 12 mg/ml) and the molecular mass of the protein sample. Measurements were performed at 20°C. Data reduction, which included normalization to beam intensity, sample transmission and detector efficiency, circular averaging and background correction, was performed with the purpose-written ILL programs RNILS and SPOLLY (Ghosh et al. 1998). The scattering curves obtained were analysed to estimate the radius of gyration (R_g) based on the Guinier approximation (Guinier and Fournet 1955) and then further examined as described below.

Solution X-ray scattering

Small angle X-ray scattering (SAXS) data were collected at Station 2.1, Synchrotron Radiation Source, Daresbury Laboratory, UK and analysed as described previously (Callaghan et al. 2003; Lu et al. 2004).

Low-resolution structure analysis

The interpretation of SANS data was performed with the ATSAS program package (Konarev et al. 2006). Distance distribution functions *p(r)* were calculated using GNOM (Svergun 1992) which provides an assessment of the maximum particle dimension (D_{max}) and the R_g value. The indirect transformation method employed in GNOM allows for a more accurate determination of R_g (including the elimination of possible concentration effects owing to the exclusion of the very beginning of the scattering profile) as long as the condition $q_{min} < \pi/D_{max}$ is satisfied (Feigin and Svergun 1987). The latter was fulfilled for all proteins considering that the largest observed D_{max} value for the catalytic domain of RNase E (170 Å) and the Tim9/Tim10 protein aggregates (90 Å, see Table 1) correspond to $q_{min} = 0.018$ and 0.035 Å^{-1}, respectively.

Ab initio low-resolution structures were calculated from the respective scattering profiles by simulated annealing

Table 1 Summary of analyses of small angle neutron scattering data

Sample	R_g (Å)	D_{max} (Å)
RNase E catalytic domain (72% D_2O)	52.8 ± 0.3	170 ± 6
RNase E catalytic domain + 5′P-RNA (72% D_2O)	49.7 ± 0.6	155 ± 5
RNase E catalytic domain + 5′OH–RNA (72% D_2O)	52.1 ± 0.2	160 ± 5
TIM10[a] (40% D_2O)	30.1 ± 0.5	88 ± 5
TIM10[a] (100% D_2O)	31.1 ± 0.5	90 ± 5

[a] Complex with deuterated subunit Tim9 and protonated subunit Tim10

with DAMMIN (Svergun 1999). For calculations concerning the catalytic domain of RNase E *D*2 symmetry was imposed as revealed by crystallographic observations. In the case of the assemblies of the two subunits (Tim9 and Tim10) within the TIM10 complex, a threefold (*C*3) symmetry constraint was introduced. This structural feature refers to the subunit composition of the complex (three copies of each of the two subunits constitute the complex) in addition to the triple internal structural repeat motif in the TIM10 substrate. Several independent shape determinations were run and the stability of the solution was inspected, the resultant shapes were aligned, averaged and filtered using DAMAVER (Volkov and Svergun 2003). We note that symmetry conditions during the computational procedure help to limit the conformational variety of shapes in order to obtain biologically meaningful models. Moreover, the experimental profiles of the RNase E catalytic domain were compared with the simulated scattering profile based on the published crystal structure (Callaghan et al. 2005) using the program CRYSON (Svergun et al. 1998). The goodness of fit value (χ) is a measure of how well the structure corresponds to the experimental data (a reliable agreement between experiment and simulation is generally obtained for $\chi < 3$). The alignment of high resolution structures with low-resolution shape models was performed with SUPCOMB (Kozin and Svergun 2001).

Results and discussion

Nucleic acid–protein complex study

Neutron scattering indicates compaction of RNase E catalytic domain upon 5′monophosphate–RNA binding but not upon 5′OH–RNA binding.

Small angle neutron scattering was used to examine the conformational changes in RNase E catalytic domain upon RNA binding in solution. With this method, the scattering contributions of the protein and RNA can be distinguished through contrast variation of the bulk solvent. The contrast agent is deuterated water, and profiles were recorded at 72% D_2O buffer composition, which corresponds to the nucleic acid match point. We used RNA with 2′*O*-methyl modification of the sugar to prevent substrate turnover. The radius of gyration of RNase E catalytic domain changes from 52.8 ± 0.3 Å, in the absence of bound RNA, to 49.7 ± 0.6 Å, in the presence of 5′ monophosphate–RNA (Fig. 2a). The distance distribution functions evaluated for the 5′ monophosphate–RNA bound and unbound states of RNase E catalytic domain also reveal subtle differences (Fig. 2a inset) indicating a more compact shape upon 5′ monophosphate–RNA binding. Thus, RNase E catalytic domain compacts upon addition of 5′ monophosphate–RNA. For the complex of RNase E catalytic domain with 5′ OH-RNA bound, the radius of gyration is close to that of the RNA-free form, 52.1 ± 0.2 Å. These data suggest that RNase E catalytic domain undergoes little structural change upon 5′OH–RNA binding and that the greatest compaction requires the 5′ monophosphate group on the RNA. The values for R_g and D_{max} for the samples of RNase E catalytic domain alone, RNase E catalytic domain bound to 5′ monophosphate–RNA and RNase E catalytic domain bound to 5′ OH–RNA are summarized in Table 1.

Ab initio shape reconstructions have been performed for the SANS data measured at the RNA match point condition (72% D_2O) to investigate the low-resolution conformation of the protein either in the absence or presence of RNA. More than 20 independent shape restorations have been carried out for each of the three protein states, averaged and filtered to produce an overall picture of the characteristic conformation in solution. The calculations were helped by the known crystal structure (e.g. the characteristic *D*2 symmetry was introduced as a constraint in the computations). The proximity measure between shapes as defined by the nominal spatial discrepancy (NSD, Kozin and Svergun 2001) displayed comparable variation for the compact 5′ monophosphate–RNA bound state (1.232 ± 0.035) against the other two protein forms (5′ OH–RNA, 1.331 ± 0.069 and RNA-free, 1.248 ± 0.103) emphasizing the consistency of the average shape representations. The results confirm the interpretation of a conformational switch based on the radii of gyration (see Fig. 2b). Whereas the 5′ monophosphate–RNA bound state matches neatly the compact conformation observed in the crystal structure, both the 5′ OH–RNA bound and RNA-free states reveal significant extensions to the shapes in the periphery of the molecule in agreement with the proposed mobility of the S1 domains in the tetrameric molecule. The close similarity of the 5′ monophosphate–RNA bound structure in solution and in crystalline state is also substantiated by scattering profile simulations (Fig. 2a). It is clear that both open conformations

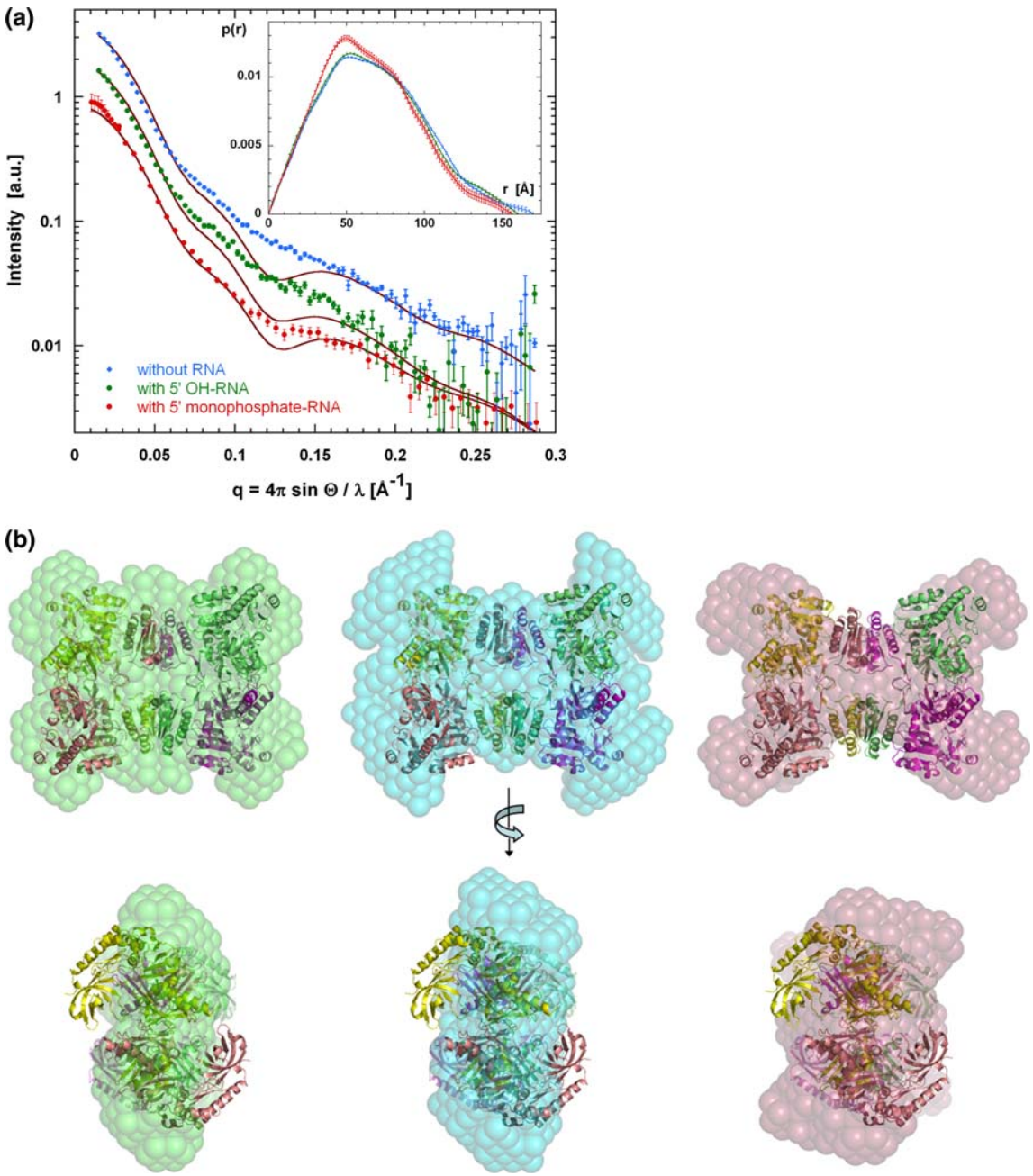

Fig. 2 Neutron scattering of RNase E catalytic domain with and without bound RNA. **a** Scattering curves *I(q)* collected at 72% D_2O contrast are shown for samples of RNase E catalytic domain-5′ monophosphate–RNA complex (*red*), RNase E catalytic domain-5′ OH–RNA complex (*green*) and RNase E catalytic domain alone (*blue*). The solid curves represent the theoretical scattering intensities calculated from the crystallographic structure of RNase E catalytic domain (Callaghan et al. 2005) and fitted to each of the experimental data sets using CRYSON. For clarity of visualization the scattering profiles are suitably displaced along the intensity axis. The inserted panel depicts the distance distribution function, *p(r)*, which yields the maximum dimension (D_{max}) for the three different molecular forms. **b** Low-resolution ab initio models for RNase E catalytic domain deduced from SANS experiments carried out at the RNA contrast match point (72% D_2O) for the RNA-free molecule (*right*, *red*) and the two RNA bound states, i.e. with 5′ OH–RNA (*centre*, *blue*) and 5′ monophosphate–RNA (*left*, *green*). Each shape is shown in two orthogonal orientations and for size comparison a ribbon model of the crystal structure of the protein in complex with 5′ monophosphate-RNA (pdb code 2B × 2) is superimposed. For clarity, the RNA was removed from the model

characterized by "X-like" shapes (Fig. 2b, blue and red) cannot be reliably fitted using the compact crystal structure. The resultant fit is very good in the case of 5′ monophosphate–RNA as substrate ($\chi = 2.0$) but significantly worse for 5′ OH–RNA ($\chi = 8.9$) and without RNA ($\chi = 13.0$).

Neutron scattering data were also collected at 43% D_2O buffer composition which corresponds to the match point

for the protein component. The profile indicates a broad peak at intermediate scattering angles (data not shown), but the signal-to-nose ratio of these data was not sufficient to confirm reliably this average distance among bound RNA moieties within the RNA-protein complex.

X-ray scattering of the RNase E catalytic domain with and without 5′OH–RNA

X-ray solution scattering data were obtained for RNase E catalytic domain in the presence of the 5′OH–RNA and compared with the unbound, apo-state of the protein (Fig. 3).

The conventional shape reconstruction approach for the apo-RNase E catalytic domain tetramer (Callaghan et al. 2003) (which is based on a two-phase system, i.e. protein and solvent) cannot be used for protein-RNA complexes because the additional phase (i.e. the nucleic acid) has a different average X-ray scattering factor compared with protein. However, in scattering profiles of RNase E catalytic domain with and without 5′OH–RNA bound the low-angle regions are almost identical indicating no large-scale

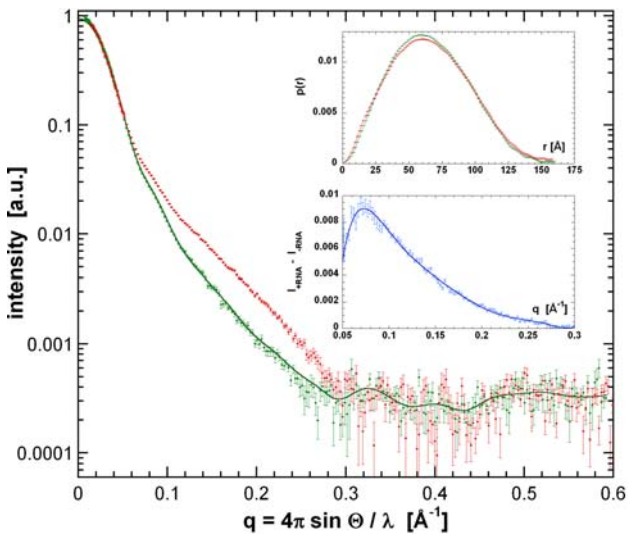

Fig. 3 Solution X-ray scattering profiles of RNase E catalytic domain with and without 5′ OH–RNA bound. The X-ray scattering profiles are shown for RNase E catalytic domain alone (*green*) and with bound 5′ OH–RNA (*red*). The smooth line represents the scattering profile of the tetramer with D2 symmetry restored from the RNA-free data (Callaghan et al. 2003). A shape cannot be calculated directly for the 5′ OH–RNA-RNase E catalytic domain complex because of the different scattering contribution of three components (solvent, protein and RNA, see text). The upper inset shows the probability distribution for the distances between scattering centres within the 5′ OH–RNA bound and unbound molecules (*red* and *green*). The intensity and distance distribution function are normalized and the area under *p(r)* was scaled to unity. The lower inset shows the difference in intensity between 5′ OH–RNA-bound and RNA-free forms, with error bars. The fitted curve (*blue*) here is not from a model but is merely a smoothed fit to the data

conformational changes to occur upon 5′OH–RNA binding. This is confirmed by the similar structural parameters obtained for the 5′OH–RNA-bound and unbound forms [Table 2: 5′OH–RNA bound RNase E catalytic domain: $R_g = 51.6 \pm 0.3$ Å, $D_{max} = 158 \pm 5$ Å; RNase E catalytic domain alone $R_g = 51$ Å with a maximal dimension of 160 Å (Callaghan et al. 2003)] as well as the very similar *p(r)* functions (Fig. 3, upper inset). The SANS and SAXS methods differ in estimated radii of the RNA-free form of RNase E catalytic domain (52.8 vs. 51.0 Å, Tables 1 and 2), but this may be due to effects of 72% D_2O present in the SANS sample. Nonetheless, the two scattering methods agree that 5′OH-RNA does not trigger substantial domain compaction.

RNA scatters more strongly than the protein, giving an additional scattering signal in the intermediate-angle scattering range (0.05 Å$^{-1} < q < 0.3$ Å^{-1}). Assuming a negligible conformational change in RNase E catalytic domain upon 5′OH–RNA binding, as supported by the neutron scattering analysis (see above), the RNA-free data can be estimated as the background signal for the 5′OH–RNA-bound dataset. This approximation is valid in the low-resolution limit of the measurements and a subtraction therefore yields the 5′OH–RNA scattering contribution (Fig. 3, lower inset). This shows a peak in the low angle region around $q \approx 0.073$ Å^{-1} which results primarily from the interference between RNA molecules bound to the RNase E catalytic domain tetramer. The q value at the peak corresponds to a distance of ~86 Å, which suggests the average centre-of-mass distance between 5′OH–RNA molecules in the tetramer is in the range 80–90 Å. In fact, this distance is the average of the inter-molecular separations of bound RNA moieties and is analogous to the difference Patterson function in X-ray diffraction from crystalline specimens, except that in this case, it is spherically averaged. Presumably the distance observed reflects the spherically averaged and contrast-weighted average of RNA-to-RNA vectors in the putatively "open" conformation of the RNase E catalytic domain tetramer. The expected mean RNA-to-RNA separation in the closed form of RNase E catalytic domain with a 5′ monophosphate–RNA bound is 71.7 Å, based on the X-ray crystal structure. This is smaller than the estimated separation of 80–90 Å between 5′OH–RNA molecules, supporting our proposal that the 5′ monophosphate–RNA

Table 2 Summary of analysis of X-ray solution scattering data

Sample	R_g (Å)	D_{max} (Å)
RNase E catalytic domain (Callaghan et al. 2003)	51.0 ± 0.3	160 ± 5
RNase E catalytic domain + 5′OH–RNA	51.6 ± 0.3	158 ± 5

favours a more compact state for the RNase E catalytic domain tetramer.

In summary, the crystal structure of RNase E catalytic domain bound to 5′monophosphate–RNA substrate analogue shows that the catalytic site and 5′ sensing site are physically separated, and yet they must somehow communicate so that the status of the 5′ end of the substrate is relayed to the active site. It has been proposed that this communication is mediated through an allosteric change in the protein (Callaghan et al. 2005). This proposed mechanism involves the engagement of the 5′ monophosphate of the RNA such that it organizes the 5′ sensor pocket, which in turn interacts with the S1 domain and causes it to clamp down on the RNA downstream, thus orienting the phosphate backbone to favor the in-line attack on the scissile phosphate by the magnesium-coordinated, activated hydroxyl group at the active site (Fig. 1c). The allosteric change suggested by this proposal is supported by our data from neutron solution scattering with contrast variation and from X-ray solution scattering analyses. We observe that only the binding of 5′ monophosphate–RNA reduces the overall dimensions of the protein illustrating 5′ monophosphate–RNA induced compaction of the protein. A likely region for the conformational change is the S1 RNA-binding subdomain of RNase E, which may lie exposed on the periphery of the tetrameric assembly, where they may contact the RNA. This is consistent with results from protease digestion patterns (Callaghan et al. 2003), which indicate that the S1 domains are linked flexibly to the core of the protein. The movement of the S1 domains would explain the compaction of the molecule upon 5′ monophosphate–RNA binding and also the observation that this subdomain is highly mobile (Callaghan et al. 2003).

Multi-protein complex study

Neutron scattering helps to delineate the subunit arrangement in the heterohexameric TIM10 complex

In order to obtain information on the spatial relationship of subunits Tim9 and Tim10 within the TIM10 complex, deuterated Tim9 was reconstituted with protonated Tim10 to form a fully functional complex made up of three copies of each subunit. Subsequently neutron contrast variation studies enabled us to look at the individual scattering contributions of the two subunits. Preliminary results of this study have been reported recently (Grossmann 2007). Here we present the experimental scattering profiles measured at 40 and 100% D_2O/H_2O buffer mixtures (Fig. 4a). Whereas the former contrast point corresponds predominantly to the scattering of Tim9 (match point for the hydrogenated protein constituent), the latter primarily suppresses the scattering from the deuterated protein component and therefore the scattering from Tim10 dominates. The finding that both scattering profiles have comparable features is underlined by very similar structural parameters (see Table 1 for R_g and D_{max} values). Tim9 and Tim10 consist of 89 and 90 residues, respectively, with primarily helical secondary structure. However, the construct used for Tim10 in this study, had an additional 29 residues attached to its N-terminal. Nevertheless, the structural resemblance between Tim9 and Tim10 is apparent, even though the two Tim subunits share only 21% sequence identity, and was investigated further by shape analysis.

More than ten independent shapes (with threefold symmetry constraint) were restored ab initio from the neutron scattering profiles and their subsequent averaging produced representative conformations for both Tim9 and Tim10 (Fig. 4b). The mean NSD values for both Tim subunits were small (1.307 ± 0.063 and 1.297 ± 0.076 for Tim9 and Tim10, respectively) indicating that the shape reconstructions are stable. Comparing both Tim9 and Tim10 average shapes clearly reveals their overall similar conformations when forming part of the TIM10 assembly. With the aim of illustrating a shape outline of the complex, the individual shapes representing Tim9 and Tim10 have been arranged in Fig. 4c so as to minimize their spatial overlap and at the same time maintain the likely overall threefold symmetrical assembly. Moreover this complex composition aimed at closely preserving the overall conformation of TIM10 as deduced from X-ray scattering experiments (Lu et al. 2004). In this way a realistic spatial correlation between the subunits within the TIM10 complex is inferred. Six protrusions can be identified which are reaching out into the solvent like sensors originating alternately from the two different subunits. In the native TIM10 complex it is expected that these protrusions are of similar size and length allowing the sequestration and protection of substrate (such as the hydrophobic AAC segments) from the inter-membrane space environment during translocation.

X-ray scattering studies of the complex with N- and C-terminal truncated Tim9 and Tim10 subunits (data not shown) were inconclusive regarding the assignment of the characteristic protrusions to either subunit. Nevertheless, the neutron contrast variation study of the partially deuterated complex provided evidence that both subunits appear to have very similar molecular conformations within the complex indicating that despite their different sequences Tim9 and Tim10 are structurally closely related and a pseudo six-fold symmetry axis may actually describe the overall low-resolution shape. The recently described high resolution structure of the human chaperone complex (Webb et al. 2006) provides detailed insights into the structural intricacies of this multi-component system and confirms the symmetry produced by a six-bladed α-propeller in which each blade is made up by individual subunits in an alternate

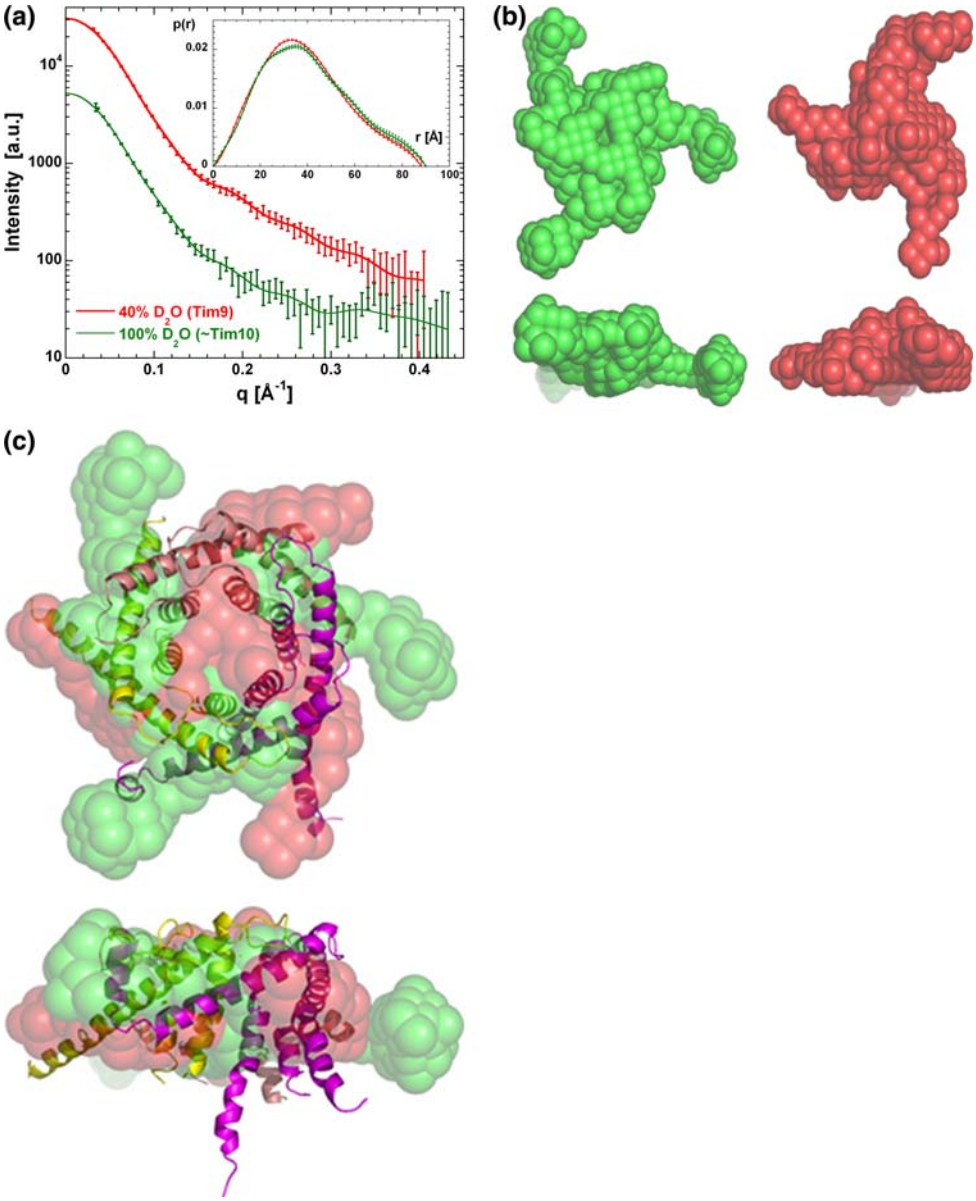

Fig. 4 Neutron scattering profiles and shape reconstructions for TIM10 complex and its subunits. **a** Neutron scattering profiles of partially deuterated TIM10 collected at 40 and 100% D_2O. The inset shows the corresponding *p(r)* functions. **b** Two orthogonal views of the average shape models restored from the SANS data for Tim9 (*red*, 40% D_2O) and Tim10 (*green*, 100% D_2O). **c** Low-resolution model arrangement of the TIM10 assembly with the individual shapes of subunits Tim9 and Tim10 coloured as in (**b**). For comparison, a ribbon model of the crystal structure of human TIM10 (Webb et al. 2006) is superimposed. Molecular graphics drawings have been produced with PYMOL (http://www.pymol.sourceforge.net)

composition of Tim9 and Tim10. Interestingly, N- and C-terminal portions of both subunits form tentacles or protrusions as observed in our low-resolution models. These are likely to be inherently more flexible in solution breaking the overall symmetry created through interacting alternating subunits in the closed circular core of the particle. The crystal structure does indeed agree very well in the core regions with our conformation deduced from the complex in solution (Fig. 4c). The regularity of the protrusions at the periphery of the molecular shape is due to the symmetry constraints applied during the shape restoration process.

Acknowledgments The work on RNase E was supported by the Wellcome Trust. We thank Martyn Symmons and Martin Moncrieffe for stimulating discussions and invaluable advice. The work on TIM10 was supported by funds from IMBB-FORTH. The ILL and STFC Daresbury Laboratory are acknowledged for beamtime. We are also very grateful to Peter Timmins at the ILL and Michael Haertlein at the ILL-EMBL-PSB Deuteration Laboratory in Grenoble for their excellent support.

References

Callaghan AJ, Grossmann JG, Redko YU, Ilag LL, Moncrieffe MC, Symmons MF, Robinson CV, McDowall KJ, Luisi BF (2003) Quaternary structure and catalytic activity of the *Escherichia coli* ribonuclease E amino-terminal catalytic domain. Biochemistry 42:13848–13855

Callaghan AJ, Marcaida MJ, Stead J, McDowall KJ, Scott W, Luisi BF (2005) Structure of E. coli RNase E catalytic domain and implications for RNA processing and turnover. Nature 437:1187–1191

Curran SP, Leuenberger D, Oppliger W, Koehler CM (2002) The Tim9p-Tim10p complex binds to the transmembrane domains of ADP/ATP carrier. EMBO J 21:942–953

Feigin LA, Svergun DI (1987) Structure analysis by small-angle X-ray and neutron scattering. Plenum Press, New York

Ghosh RE, Egelhaaf SU, Rennie AR (1998) A computing guide for small-angle scattering experiments, Institut Laue-Langevin, ILL98GH14T

Grossmann JG (2007) Biological solution scattering: recent achievements and future challenges. J Appl Cryst 40:s217–s222

Guinier A, Fournet G (1955) Small-angle scattering of X-rays. Wiley, New York

Jiang X, Belasco JG (2004) Catalytic activation of multimeric RNase E and RNase G by 5′-monophosphorylated RNA. Proc Natl Acad Sci USA 101:9211–9216

Koehler CM, Merchant S, Oppliger W, Schmid K, Jarosch D, Dolfini L, Junne T, Schatz G, Tokatlidis K (1998) Tim9p, an essential partner subunit of Tim10p for the import of mitochondrial carrier proteins. EMBO J 17:6477–6486

Konarev PV, Petoukhov MV, Volkov VV, Svergun DI (2006) ATSAS 2.1, a program package for small-angle scattering data analysis. J Appl Crystallogr 39:277–286

Kozin MB, Svergun DI (2001) Automated matching of high- and low-resolution structural models. J Appl Crystallogr 34:33–41

Lu H, Golovanov AP, Alcock F, Grossmann JG, Allen S, Lian L-Y, Tokatlidis K (2004) The structural basis of the TIM10 chaperone assembly. J Biol Chem 279:18959–18966

Mackie GA (1998) Ribonuclease E is a 5′-end-dependent endonuclease. Nature 395:720–723

McDowall KJ, Lin-Chao S, Cohen SN (1994) A+U content rather than a particular nucleotide order determines the specificity of RNase E cleavage. J Biol Chem 269:10790–10796

Pfanner N, Geissler A (2001) Versatility of the mitochondrial protein import machinery. Nat Rev Mol Cell Biol 2:339–349

Redko Y, Tock MR, Adams CJ, Kaberdin VR, Grasby JA, McDowall KJ (2003) Determination of the catalytic parameters of the N-terminal half of *E. coli* ribonuclease E and the identification of critical functional groups in RNA substrates. J Biol Chem 278:44001–44008

Svergun DI (1992) Determination of the regularization parameter in indirect-transform methods using perceptual criteria. J Appl Crystallogr 25:495–503

Svergun DI (1999) Restoring low resolution structure of biological macromolecules from solution scattering using simulated annealing. Biophys J 76:2879–2886

Svergun DI, Richard S, Koch M, Sayers Z, Kuprin S, Zaccai G (1998) Protein hydration in solution: experimental observation by X-ray and neutron scattering Proc Natl Acad Sci USA 95:2267–2272

Vergnolle MAS, Alcock FH, Petrakis N, Tokatlidis K (2007) Mutation of conserved charged residues in mitochondrial TIM10 subunits precludes TIM10 complex assembly, but does not abolish growth of yeast cells. J Mol Biol 371:1315–1324

Vial S, Lu H, Allen S, Savory P, Thornton D, Sheehan J, Tokatlidis K (2002) Assembly of Tim9 and Tim10 into a functional chaperone. J Biol Chem 277:36100–36108

Volkov VV, Svergun DI (2003) Uniqueness of ab initio shape determination in small-angle scattering. J Appl Crystallogr 36:860–864

Webb CT, Gorman MA, Lazarou M, Ryan MT, Gulbis JM (2006) Crystal structure of the mitochondrial chaperone TIM9.10 reveals a six-bladed alpha-propeller. Mol Cell 21:123–133